Macromolecules

Article

pubs.acs.org/Macromolecules

Directed Assembly of Block Copolymer Templates for the Fabrication of Mesoporous Silica Films with Controlled Architectures via 3-D Replication

Li Yao,[†] Arthur R. Woll,[‡] and James J. Watkins[†,*]

[†]Department of Polymer Science and Engineering, University of Massachusetts Amherst, 120 Governors Drive, Amherst, Massachusetts 01003, United States

[‡]Cornell High Energy Synchrotron Source, Cornell University, Ithaca, New York 14853, United States

Supporting Information

ABSTRACT: Mesoporous silica films with cylindrical or spherical pores up to 40 nm in diameter were fabricated by replicating the morphologies of polystyrene-*b*-poly(*tert*-butyl acrylate), PS-*b*-PtBA, copolymers using CO_2-assisted infusion and phase selective condensation of tetraethylorthosilicate within the polymer template. The template structures, including domain packing, orientation and spacing were controlled by adjusting the molecular weight, volume fraction and polydispersities of the block copolymers and by solvent annealing. Cylinder alignment was achieved in polymer templates through directed self-assembly (DSA). The structural details imparted to the template prior to precursor infusion were retained in the mesoporous films. In one example, aligned PS-*b*-PtBA templates were replicated to yield massively parallel arrays of cylindrical pores with pore diameters up to ~20 nm. The ability to tune pore sizes in this range within aligned nanochannels is attractive for applications involving biomolecules.

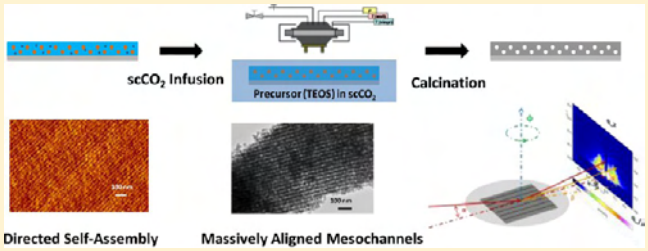

INTRODUCTION

Mesoporous metal oxide films with well-defined pore structures are of interest for many applications[1] including microelectronics,[2−6] photovoltaics,[7−10] separations,[11,12] catalysis,[13−15] absorption,[16,17] sensors,[18,19] and biomedicine.[20−22] Ultimately, the utility of the films for a specific device is predicated on the ability to match the size, shape, orientation, and potentially the long-range order of a pore structure to the specific needs of the application. To date several methods to produce well-ordered films using surfactants[23−31] such as Pluronic P123,[23] cetyltrimethylammonium (C16TMA)[30] and alkyltrimethylammonium bromides[31] have been reported. The process typically involves cooperative assembly and silica precursor condensation from aqueous or alcohol solution such that structure generation via self-assembly and silica network formation via precursor condensation occur simultaneously and are intimately linked. Consequently, the fabrication processes for films are often subject to kinetic constraints, which can complicate control of morphology during processing. Moreover, the use of low molecular weight surfactants typically yields relatively small (<5 nm) pores. Recent reports indicate mesoporous materials with relatively large pore sizes can be prepared from solution using high molecular weight block copolymers[27,32−35] swelling agents and/or discrete condensed objects[36] with surfactant or block copolymer templates, but to date these approaches have not been successfully applied to the formation of mesoporous films. A method[37] using PMMA latex nanoparticles as a sacrificial template was developed to fabricate mesoporous silica films with large pore sizes (30 nm −80 nm), however only spherical pores could be achieved using this approach.

The fabrication of mesoporous silica films with well controlled cylindrical pores is of interest for many applications including the fabrication of solid state devices for processing, separation and detection. While several reports indicate the fabrication of well controlled cylindrical pores in mesoporous films,[38−41] only relatively small pore sizes (less than or around 10 nm) have been achieved. Separation and detection of large molecules, macromolecules and biomolecules require the fabrication of meosporous silica films with cylindrical channels having much larger pore diameters.

Previously, our group reported an efficient pathway[42] to well-ordered, robust mesoporous films with tailored morphologies through the infusion and selective condensation of silica and organosilicate precursors[43] within one phase of a preformed block copolymer template dilated with supercritical carbon dioxide. The template is subsequently removed from the resulting composite via thermal degradation to produce the mesoporous oxide films. The role of the supercritical fluid in the process is 2-fold. The solubility of the silica precursor in CO_2 enables its infusion into the template and modest dilation of the

Received: May 15, 2013
Revised: July 3, 2013
Published: July 22, 2013

   dx.doi.org/10.1021/ma401018y | *Macromolecules* 2013, 46, 6132−6144

template with CO_2 enables facile diffusion of the reagents and byproducts during the silica condensation reaction[44,45] without excessive dilation, which could disrupt the desired template structure, orientation and/or morphology. This strategy has been applied to the synthesis of films with spherical pores for use as ultralow dielectric constant materials,[42] to the fabrication of films with vertically[46] and horizontally[47] oriented cylindrical nanochannels, and most recently to the direct patterning of mesoporous films without the need for etching.[48,49] One advantage of this approach compared to those that involve cooperative assembly with simultaneous silica network condensation is the separation of template organization and silica condensation into discrete steps. Such an approach enables conveyance of the structural details of template film into the silica replica. Moreover, films produced via this process exhibit low residual stress and excellent mechanical stability.[42]

The morphology and domain size of phase separated block copolymer templates is controlled by the volume fraction (f) of each block, the Flory parameter and the degree of polymerization (N).[50] Moreover, secondary details of the structure, such as domain orientation and long-range order can be enhanced or controlled using solvent annealing,[51−60] interfacial interactions,[61−66] substrate topography,[67−76] or external fields.[77−84] One of our goals is to take advantage of these pathways to fully control template structure prior to their replication in silica. In this paper we report the use of this 3-D replication approach to fabricate mesoporous silica films with large-pores and shape-controlled channels by directly replicating the morphology in preordered block copolymer films. We show that the influences of polydispersity in template molecular weight, which can increase lattice spacing of BCPs, template film thickness, which can influence domain orientation and packing within the BCPs, and solvent annealing, which can improve long-range order in the BCP are reflected in the morphologies of the mesoporous silica films derived from the template film. We also report that the use of directed self-assembly (DSA), which can be used to achieve the long-range cylinder alignment in block copolymer films,[67,85−90] can be combined with our replication strategy to create massively aligned mesochannels with tunable pore sizes up to ∼20 nm in diameter. Nanochannels in this size range are particularly attractive for applications involving biomolecules and to our knowledge these are the largest reported for well aligned cylindrical channels in mesoporous silica films.

EXPERIMENTAL SECTION

Materials. *N,N,N′,N′,N″*-Pentamethyldiethylenetriamine (PMDETA), styrene, *tert*-butyl acrylate, ethyl-2-bromoisobutyrate, anisole, copper(I) bromide, copper(II) bromide, and tetraethylorthosilicate (TEOS) (99%) were purchased from Acros Organics, and triphenylsulfonium triflate (TPST) was purchased from Sigma-Aldrich. Photoresist NR9−1000PY was purchased from Futurrex, Inc. A quartz mask with line-patterns for photolithography was obtained from Benchmark Technologies, Inc.

Block Copolymer Synthesis. Atom transfer radical polymerization (ATRP) was used for the synthesis of poly(styrene-*b*-*tert*-butyl acrylate) (PS-*b*-PtBA) diblock copolymers using established procedures with slight modification.[91] A magnetic stirbar, CuBr and $CuBr_2$ were added in a pear-shape Schlenk flask, which was dried in an oven overnight and caped with a rubber septa, evacuated and purged. Distilled styrene and PMDETA (purged with house nitrogen (N_2) for 30 min), were injected into the flask. After three freeze/pump/thaw cycles, the initiator ethyl-2-bromoisobutyrate was injected dropwise into the flask which was then heated to 90 °C for 5 h. After dilution with tetrahydrofuran (THF), the resulting dark green solution was run through a column of neutral alumina and then precipitated in excess methanol, filtered, washed, and dried. The product was used as the macroinitiator for chain extension, also performed following similar procedures with a slight modification.[91] The macroinitiator (PS), CuBr, and a magnetic stirbar were added into a Schlenk flask, followed by addition of purged anisole and distilled *tert*-butyl acrylate. After all solids were completely dissolved and three freeze/pump/thaw cycles, PMDETA was injected dropwise into the flask which was then heated for 48 h at 60 °C. The same purification procedure as the first step was performed to give a white solid.

Formation of Patterned Substrates. The photoresist used in the process is NR9−1000PY, a negative lift-off resist. Spin-coating was performed on a Brewer Science CEE 100CB Spin Coater with the spinning rate 3000 rounds per minute (rpm) for 60 s using silicon wafers (type-doping, N/Sb; orientation, ⟨111⟩) as substrates. Pre-exposure baking was set at 150 °C for 60 s.

Photolithography was performed on a SUSS MA6Mask Aligner with a quartz mask containing line-patterns. The UV exposure time was 30 s with intensity of 388 mJ/cm^2. The post exposure bake was conducted at 100 °C for 60 s. The substrates were then developed in the RD6 developer for 12 s, rinsed with distilled water and then dried in N_2.

Reactive ionic etching (R.I.E.) was performed on a STS Vision 320 Reactive Ion Etch system. CF_4 plasma was used for silicon etching with the process pressure of 5 mT, the RF set point at 100 W, the stabilization time for 15 s, the CF_4 flow at 30 sccm. The etching rate for silicon was ∼9.24 nm per minute measured by AFM (see Supporting Information).

Formation of Polymer Film Templates. Polymer films with thickness of 350 nm were spin-coated from a 3−5 wt % solution of PS-*b*-PtBA prepared in chloroform with 5 wt % TPST (to polymers) onto silicon wafers or patterned substrates at 3000 rpm for 60 s. To achieve different thickness films, the spin-coating solution was diluted or concentrated. The template film cast on the silicon wafer was then annealed under chloroform vapor in a bell jar prior to infusion.

Infusion of Silica Alkoxide Precursors. The templates were subject to UV flood exposure (254 nm) at room temperature for 20 s with 40 MJ/cm^2 and then sealed inside of a 150 mL stainless steel reactor containing 10 μL of TEOS. At room temperature, 62 mL of CO_2 with the pressure of 68.9 bar at room temperature was injected into the reactor. The reactor was then heated to 60 °C for 2 h at a pressure of 103 bar. The composite was removed from the reactor and a uniform mesoporous silica film was generated by calcination at 400 °C for 6 h in air using a temperature ramp rate of 1.56 °C/min.

Characterization. Gel permeation chromatography (GPC) was performed in THF at a flow rate of 1.0 mL/min using polystyrene as standards. 1H NMR spectra were acquired on a Bruker DPX300 NMR spectrometer (300 MHz) in deuterated chloroform. Atomic force microscopy (AFM) topographic and phase images were acquired on a Digital Instruments Dimension 3000 scanning microscope in tapping mode. A profilometer (Dektak3) and a Filmetrics Optical Profilometer were used to measure the thickness of the films.

Transmission electron microscopy (TEM) was performed on a JEOL 2000FX electron microscope operating at 200 kV. The mesoporous silica films were scraped off the substrates using a razor blade and ground to form a dilute slurry in ethanol. The suspension was dropped onto Formvar coated copper grids (Electron Microscopy Sciences), which was then dried in air prior to imaging.

Grazing incidence small-angle X-ray scattering (GISAXS) experiments were performed at the G1 station of the Cornell High Energy Synchrotron Source (CHESS). For Figure 2, 3, 5, 6, and 7, the wavelength of X-rays used was 1.4617 Å and the sample to detector distance was 2572.1 mm. For Figure 11 and 12, the wavelength of X-rays used was 1.4653 Å and the sample to detector distance was 2399.7 mm. The angle of incidence was chosen to be above the critical angle of the film under study. A two-dimensional charge-coupled device (CCD) camera with image sizes of 1024 pixels by 1024 pixels was used to collect the scattered radiation. The GISAXS 1D profiles were all based on the integration of line scans in $q_{\|}$ axes.

RESULTS AND DISCUSSION

Block Copolymer Synthesis and Template Formation. Poly(styrene-*b*-*tert*-butyl acrylate) (PS-*b*-PtBA) copolymers of

dx.doi.org/10.1021/ma401018y | *Macromolecules* 2013, 46, 6132−6144

Table 1. Characteristics of PS-*b*-PtBA Templates Used in this Study and Characteristics of the Corresponding Mesoporous Silica Films Prepared using the Templates

polymer templates						mesoporous silica films		
sample	M_n(PS)	M_n(PtBA)	total	PtBA wt %	PDI	morphology	*d*-spacing[a] (nm)	pore size[b] (nm)
P1	28K	125K	153K	81.7	~1.5	spherical	76	~40
P2	23K	100K	123K	81.3	~1.33	spherical	62	~37
P3[c]	19K	69K	88K	78.4	1.07	cylindrical	40	~22
P4	11.4K	32.7K	44.1K	74.1	1.3	cylindrical	38	~20
P5	11.4K	37.9K	49.3K	76.9	1.21	cylindrical	35	~17

[a]Calculated from GISAXS data. [b]Estimated from TEM images. [c]Acquired from Polymer Source by anionic polymerization. All others synthesized by ATRP.

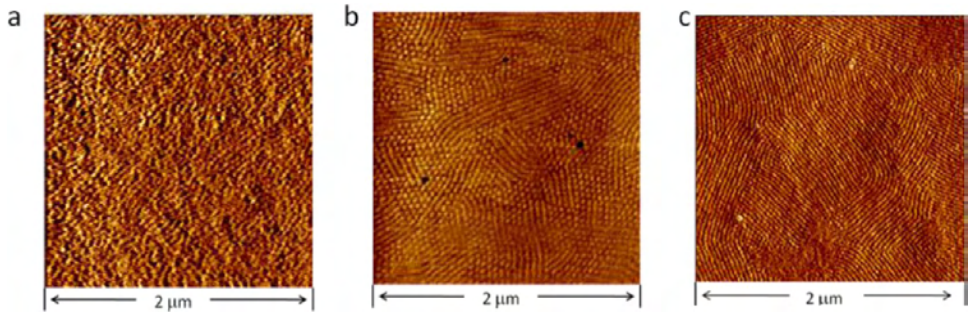

Figure 1. AFM Images of PS-*b*-PtBA film (P5, 49.3K PS-*b*-PtBA, 76.9% PtBA, PDI = 1.21) before and after solvent annealing. (a) As-spun film. (b) Film annealed under saturated chloroform atmosphere for 4 h. (c) Film annealed under dilute chloroform vapor (200 μL chloroform in a 250 mL jar) for 15 h.

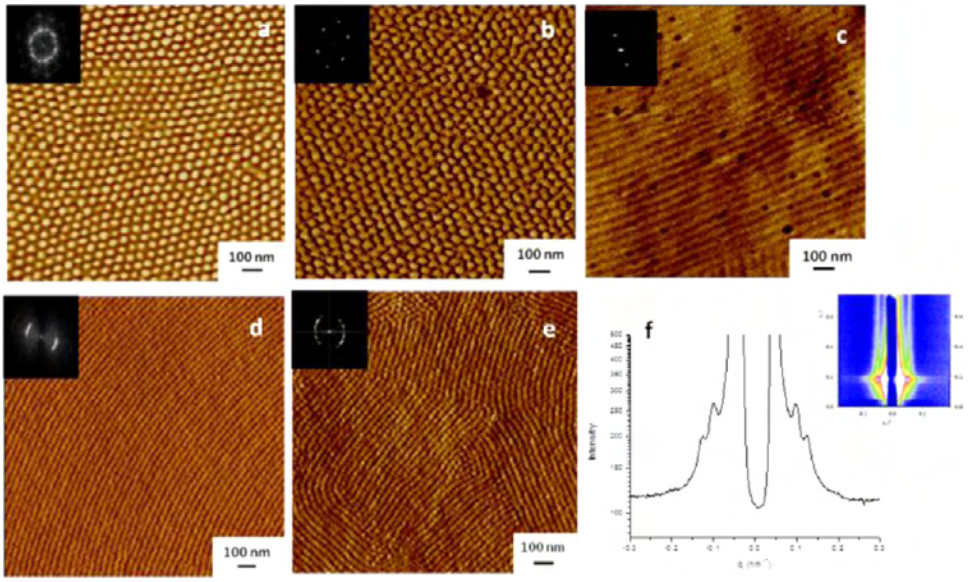

Figure 2. AFM phase images (a–e) for PS-*b*-PtBA films with film thicknesses of 400 ± 50 nm after chloroform annealing: (a) P1 (153 K PS-*b*-PtBA, 81.7% PtBA, PDI = 1.5) after solvent annealing for 24 h in saturated chloroform vapor; (b) P2 (123 K PS-*b*-PtBA, 81.3% PtBA, PDI = 1.33) after 24 h in dilute chloroform vapor (250 μL chloroform in a 250 mL jar); (c) P3 (88K PS-*b*-PtBA, 78.4% PtBA, PDI = 1.07) after annealing for in saturated chloroform vapor; (d) P4 (44.1K PS-*b*-PtBA, 74.1% PtBA, PDI = 1.3) after annealing for 15 h in dilute chloroform vapor (200 μL chloroform in a 250 mL jar); (e) P5 (49.3K PS-*b*-PtBA, 76.9% PtBA, PDI = 1.21) after annealing in dilute chloroform vapor (200 μL chloroform in a 250 mL jar). (f) GISAXS spectrum and integration for P2 shown in part b.

tailored molecular weight and volume fraction were used as templates (Table 1). Except for P3, all the polymers from Table 1 were synthesized by atom transfer radical polymerization (ATRP) at molecular weights ranging from 44K to 153K.

We first investigated how improvements in microphase segregation and the degree of order imparted to the PS-*b*-PtBA templates via solvent annealing in the presence of chloroform impacted the morphology of the mesoporous films. Chloroform, which exhibits a solubility parameter, δ(SI), of 18.7 is a good solvent for both PS and PtBA. We used two annealing protocols. In the first, the template films were annealed in saturated chloroform vapor at room temperature for 4 h. The second protocol involved annealing in dilute chloroform vapor (200 μL chloroform in a 250 mL jar) for 15 h at room temperature. Figure 1a shows an AFM phase image of a 400 ± 30 nm thick film of 49.3K PS-*b*-PtBA containing a PtBA weight percentage of ~77% (Table 1, P5) prepared by spin coating from a 3 wt % solution of the copolymer in chloroform. The image (Figure 1a) suggests

dx.doi.org/10.1021/ma401018y | *Macromolecules* 2013, 46, 6132–6144

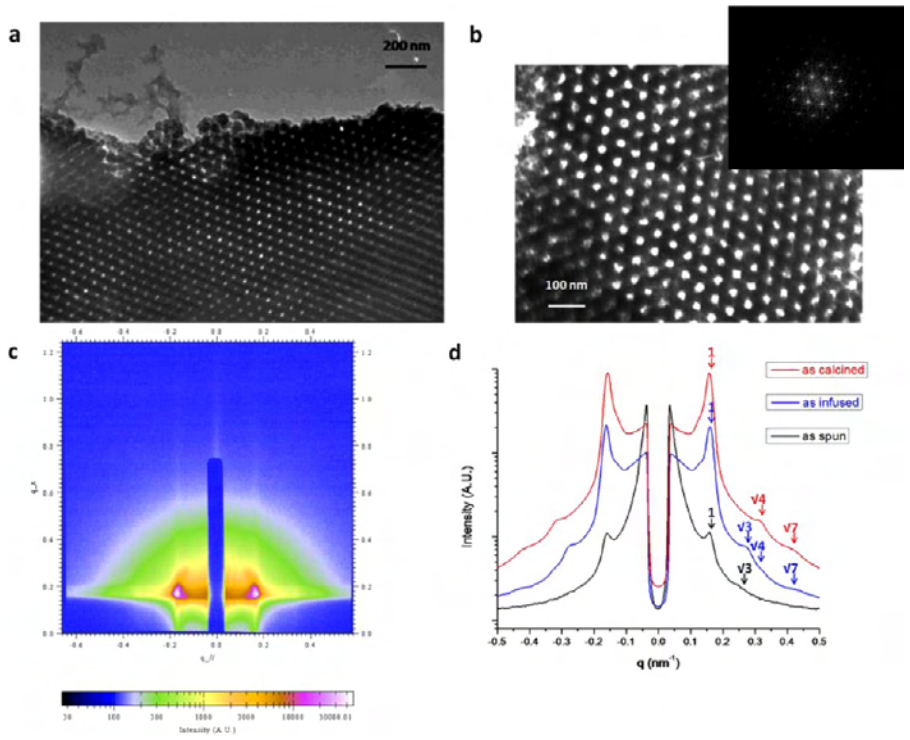

Figure 3. Characterization of mesoporous silica film templated from P3 (88K PS-*b*-PtBA, 78.4% PtBA, PDI = 1.07). (a, b) TEM images; image b is shown with its Fourier transform. (c) GISAXS analysis of the film. (d) Integration of the GISAXS data for the as-spun PS-*b*-PtBA film, the as infused polymer/silica composite film and the calcined mesoporous silica film.

poor microphase segregation and weak order in the as spun template. Figure 1b is an image of the film after annealing in saturated chloroform vapor for 4 h at room temperature, which yielded a cylindrical morphology with grains containing cylinders oriented perpendicular or parallel to the substrate. Figure 1c shows an image of films after annealing in dilute chloroform vapor for 15 h. These annealing conditions resulted in a cylindrical morphology in which the domains are primarily oriented parallel to the substrate.

Similar chloroform annealing methods were applied to other PS-*b*-PtBA films with different molecular weights and PtBA volume fractions to give well-ordered structures, as shown in Figure 2. The thicknesses of these films are in the range of 400 ± 50 nm, which are about 6 times larger than their *d*-spacings. Block copolymers P1 and P2 from Table 1 exhibited spherical morphologies, as shown in parts a and b of Figure 2, while P3, P4, and P5 exhibited cylindrical morphologies as shown in parts c−e of Figure 2. Table 1 shows the morphologies of polymer templates as well as the *d*-spacings and approximate pore dimensions of the mesoporous silica films fabricated using each of the templates. Templates with spherical pore morphologies and ∼75 nm and ∼64 nm *d*-spacings were prepared using P1 and P2 respectively (Figure 2a,b). Films prepared using block copolymer P1 (M_n = 153K, PDI = 1.5) exhibited poor order, while films prepared using P2, (M_n = 123K, PDI = 1.33) exhibited a face-centered cubic FCC morphology with a *d*-spacing of 64.1 nm as confirmed using grazing-incidence small-angle X-ray scattering (GISAXS) (Figure 2f).

Mesoporous Silica Film Fabrication using BCP Templates. The use of supercritical fluid assisted infusion and phase selective condensation of metal oxide precursors to fabricate mesoporous films is described in detail elsewhere.[42,48,49,92,93] Here, we show that the use of CO_2 dilation enables silica condensation within well-ordered PS-*b*-PtBA template films with molecular weights (44.1K−153K) yield large-pore (17−40 nm) silica films. The photoacid generator triphenyl sulfonium triflate (TPST) was used to generate acid within the template upon exposure to UV-light (254 nm). The chemical amplification process and tetraethyl orthosilicate (TEOS) infusion occur simultaneously within the supercritical carbon dioxide reactor to convert the PtBA domain into poly(acrylic acid)(PAA) and to initiate silica condensation selectively within the hydrophilic PAA-rich matrix to form a polymer/silica composite film at 60 °C and 105 bar. The mesoporous silica films were obtained by removal of the template via calcination. We point out that the use and deprotection of PS-*b*-PtBA templates offers distinct advantages to the direct use of PS-*b*-PAA as template. These include ease of solubility and spin-coating of the template and the relatively low T_g of the PtBA block relative to PAA, which facilitates achievement of well-ordered films during thermal annealing and the infusion of the silica precursor during the SCF exposure step. The morphology of mesoporous films prepared from templates of PS-*b*-PtBA was investigated using transmission electron microscopy (TEM) and GISAXS.

Figure 3 shows the mesoporous silica film obtained using PS(19K)-*b*-PtBA(69K) as the template (P3, Table 1). TEM imaging suggests a cylindrical morphology with hexagonal packing (Figure 3a,b) and a pore diameter of ∼22 nm. GISAXS confirmed the morphology and revealed a *d*-spacing of 40 nm (Figure 3c,d). GISAXS was also used to compare the as-infused and as-spun films. There is no obvious difference of the *q* values of the first order peak in all three films indicating little influence of swelling or shrinkage during the process. The increase in peak intensity from the as-spun to as-infused, to calcined films evident in Figure 3d is as expected due to increasing electron density

dx.doi.org/10.1021/ma401018y | *Macromolecules* 2013, 46, 6132−6144

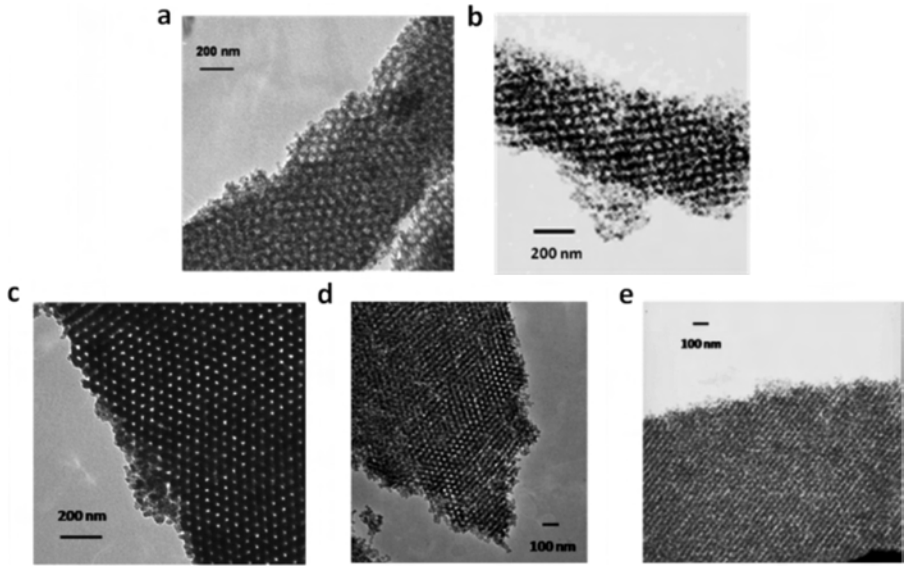

Figure 4. TEM images of mesoporous silica films templated from templates (a) P1, (b) P2, (c) P3, (d) P4, and (e) P5 in Table 1 and Figure 2.

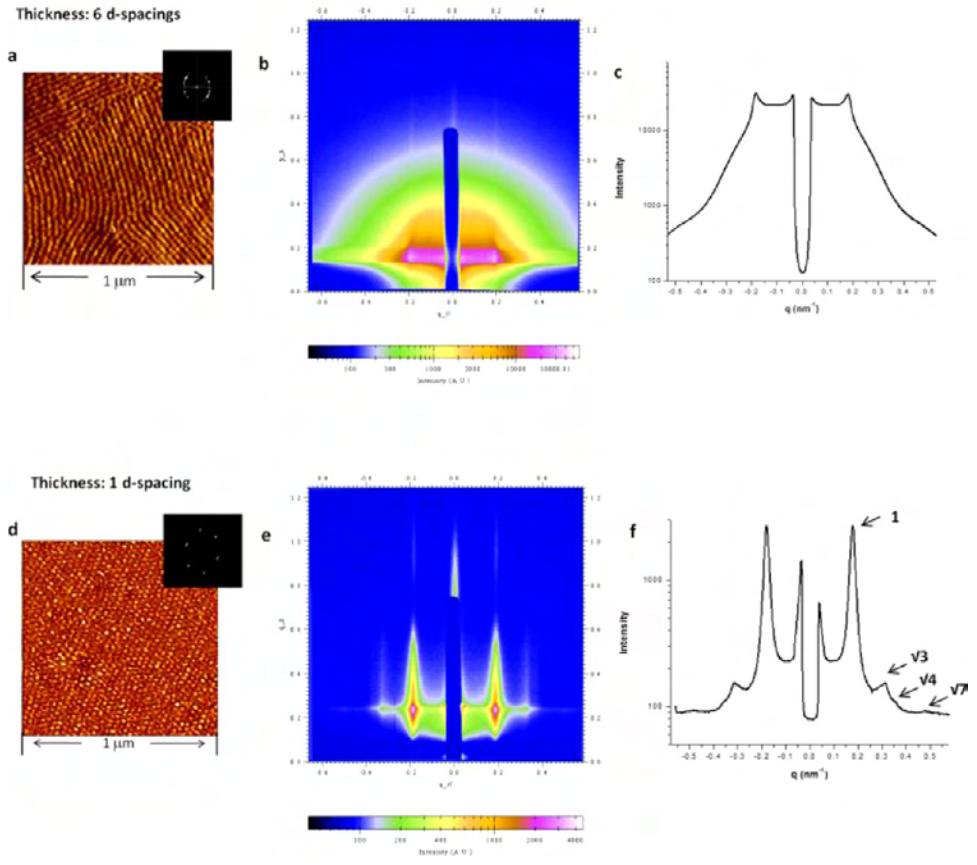

Figure 5. Influence of template thickness on the morphologies of the template P5 (49.3K PS-*b*-PtBA, 76.9% PtBA, PDI = 1.21) annealed in dilute chloroform vapor for 15 h and corresponding mesoporous silica films for template thicknesses equivalent to 6 *d*-spacings or 1 *d*-spacing. (a) AFM image of template with thickness of 6 *d*-spacings, (b) GISAXS spectrum ,and (c) GISAXS 1D integration line profile of mesoporous film in $q_{||}$ derived from part a. (d) AFM image of template with thickness of ∼1 *d*-spacing. (e) GISAXS spectrum and (e) GISAXS integration of mesoporous film derived from part d.

contrast in the silica/polymer composite and the mesoporous silica film relative to the PS-*b*-PtBA template.

A similar supercritical fluid assisted infusion process was applied to other ordered PS-*b*-PtBA templates (shown in Figure 2) to generate mesoporous silica films with well-ordered structures and tunable pore sizes and shapes (Figure 4, Table 1). We note here that while pore diameters and *d*-spacings of the mesoporous films can be controlled by varying the molecular weight of the polymer templates, the final mesoporous film dimensions are also influenced by the mass uptake of silica during

dx.doi.org/10.1021/ma401018y | *Macromolecules* 2013, 46, 6132−6144

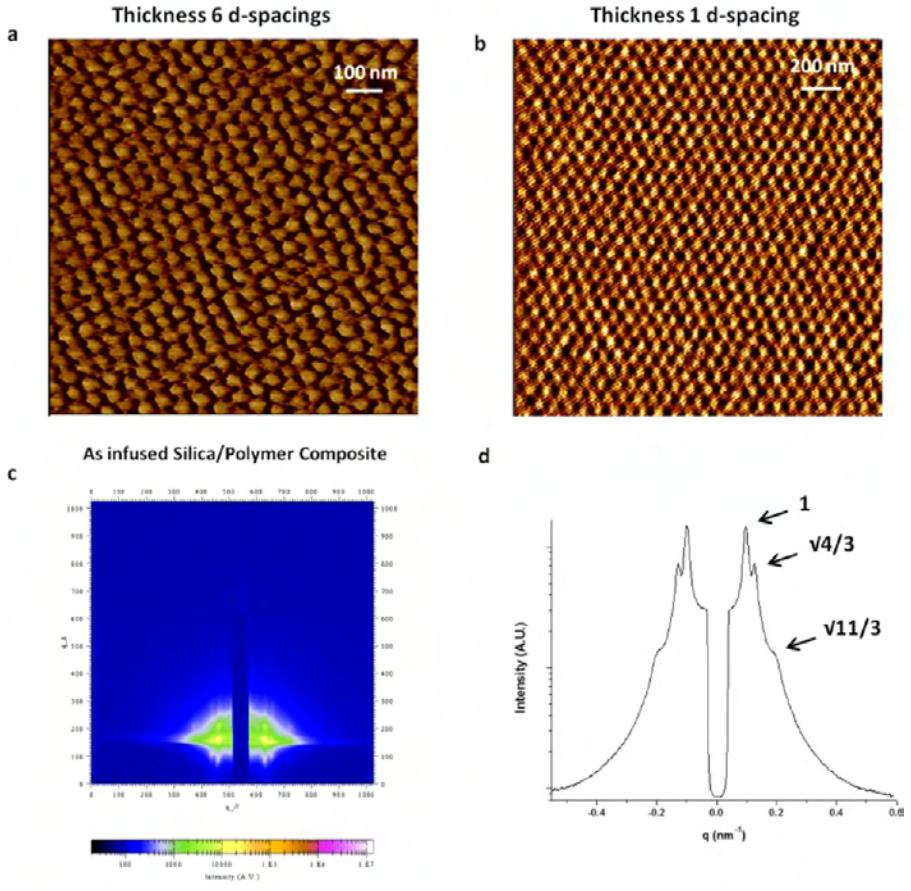

Figure 6. Influence of template thickness on sphere packing in the template film and in the corresponding mesoporous silica film. AFM phase images for P2 (123 K PS-*b*-PtBA, 81.3% PtBA, PDI = 1.33) with the thickness equivalent to ~6 *d*-spacings (a) and 1 *d*-spacing (b). (c) GISAXS spectrum and (d) its integration for silica/polymer composite prepared from the sample shown in part a.

fabrication and silica network contraction during calcination. Parts a and b of Figure 4 show mesoporous silica films with *d*-spacings of 76 and 62 nm, respectively. The 40 nm pores shown in Figure 4a are to our knowledge the largest reported in a mesoporous silica film. GISAXS measurements were used to confirm the morphologies and *d*-spacings and to provide clear information about the morphology over large areas on the film surface (see Figures S1, S2, S3, S4, and S5, Supporting Information) As shown in Figure 4 and Table 1 similar *d* spacings of ~40 nm (P3, P4) were templated from two block copolymers with very different molecular weights of 88K and 44K respectively. The two BCPs were synthesized using different methods, which yield large differences in PDI. The BCP (P3) was synthesized by anionic polymerization and was purchased from Polymer Source while the BCP (P4) was synthesized by ATRP as shown in the Experimental Section. The relatively large polydispersity of the template block copolymers produced by ATRP gave rise to larger *d*-spacing relative to narrow PDI samples of the same molecular weight. These larger template *d*-spacings are reflected in the mesoporous films. Self-consistent field theory has been used to quantitatively explain this phenomenon.[94−96]

Influence of Template Film Thickness on Cylindrical Pore Orientation. It is well-known that the domain orientation in block copolymer films cast on solid substrates is influenced by both surface interaction and the thickness of the film. AFM and GISAXS analysis shown in Figure 5 indicates that for a PS(11.4K)-*b*-PtBA(37.9K) copolymer exhibiting a cylindrical morphology (P5 in Table 1) cast onto the native oxide of a Si wafer with a film thickness equivalent to 6 or 12 times the domain spacing, the cylinders are oriented parallel to the substrate. As the thickness decreases toward that equivalent to a single layer, the cylinders are oriented perpendicular to the substrate with hexagonal packing (Figure 5d). The influence of film thickness on domain orientation was experimentally investigated by van Dijk[97] and theory developed by Lee.[98] For very thin films in the absence of strong preferential interactions of the surface with one of the blocks, conformational entropy energy dominates the total free energy, leading to vertical orientation of the cylinders. For films whose thicknesses are large relative to domain spacing, two degrees of orientational freedom are available in a parallel morphology.[97,98] Thus, the parallel cylinder orientation is favored in a thick film, while perpendicular orientation is favored in a thin film. GISAXS analysis confirmed that these orientations are maintained during the template replication process in supercritical carbon dioxide and are subsequently conveyed to the mesoporous silica films. As shown in the thick film (Figure 5b,c), the first order peak gives a *d*-spacing of ~35 nm and the weak intensity is consistent with weak in-plane ordering. While, in the thin film (Figure 5e), the sharp scattering rods along the q_z axis vertical to $q_{||}$ axes indicate the vertical cylinder orientation and the higher order peaks at $\sqrt{3}$, $\sqrt{4}$, and $\sqrt{7}$ multiples of the location of the first order peak confirm a cylindrical morphology with in-plane hexagonal packing exhibiting a *d*-spacing equivalent to those found in the thicker films containing pores oriented parallel to the surface.

dx.doi.org/10.1021/ma401018y | *Macromolecules* 2013, 46, 6132−6144

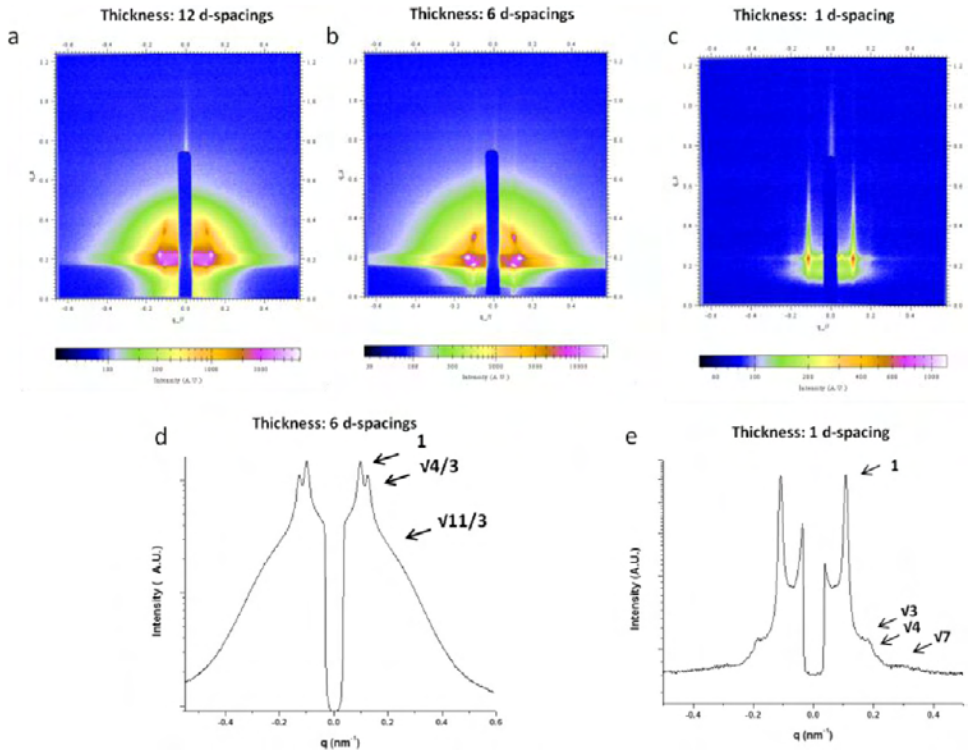

Figure 7. (a–c) GISAXS spectrum and (d, e) GISAX integrations for mesoporous silica film templated from P2 (123 K PS-*b*-PtBA, 81.3% PtBA, PDI = 1.33) at thickness equivalent to 12 *d*-spacings, 6 *d*-spacings, and 1 *d*-spacing.

Influence of Template Film Thickness on Spherical Pore Packing. BCPs with spherical morphologies can exhibit BCC or FCC packing. While BCC morphologies are common, the FCC morphology in neat block copolymers has been theoretically studied[98,100] but is not often observed experimentally because of its narrow temperature window within the phase diagram,[99,101] strong thermal fluctuations under experimental conditions,[102,103] or competition with the disordered micelle regime.[104] In the work presented here, BCPs with high PDIs and high molecular weight, synthesized by ATRP, have larger FCC windows relative to copolymers with narrow PDI and the FCC morphology can be kinetically trapped during solvent annealing.[105,106] For the block copolymer (PS23K-*b*-PtBA100 K, P2 in Table 1) cast on the native oxide of a silicon wafer with a thickness equivalent to 6 *d*-spacings, an FCC spherical morphology was confirmed by AFM measurement of template morphology (Figure 6a) and GISAXS measurement (Figure 2f).

The influence of film thickness on spheres packing in the polymer template PS-*b*-PtBA films (PS23K-*b*-PtBA100 K, P2 in Table 1) has also been observed. As the thickness decreased to a monolayer, the spherical pores pack into a hexagonal array was confirmed by AFM (Figure 6b). Because of the packing frustration,[107] the hexagonal Wigner–Seitz (W–S) cell of sphere monolayer has a relatively smaller free energy increase to make the transition from FCC to hexagonal packing possible when the thickness decreases to a monolayer.

Supercritical CO_2 infusion was then applied to convey the influence of film thickness on sphere packing within polymer template to pore packing within mesoporous silica films. The FCC packing was confirmed by higher order peaks, $\sqrt{4/3}$ and $\sqrt{11/3}$, in GISAXS analysis for as-infused silica/polymer composite films with 6 *d*-spacings (Figure 6d). As for mesoporous silica films after calcination, three thicknesses of 12 *d*-spacings, 6 *d*-spacings and 1 *d*-spacing have been investigated in this study by GISAXS, and the results are shown in Figure 7, parts a–c. The 12 *d*-spacings and 6 *d*-spacings gave similar scattering results that were assigned to spherical pores with FCC packing, while the 1 *d*-spacing gave $\sqrt{3}q$ as the first high order peak in GISAXS results, indicating the hexagonal packing.

Directed Assembly of Block Copolymer Templates for the Fabrication of Aligned Mesochannels in Silica Films. To fabricate well aligned mesochannels in silica films for applications including microfluidics and biomolecule seprartions, cylinder alignment in the block copolymer templates needs to be achieved. Long-range alignment in block copolymer films has been widely investigated and can be achieved by directed self-assembly (DSA), using larger period length patterns on the substrate to direct the long-range alignment in block copolymer films with smaller *d*-spacings.[85] Typically, either topographic guiding patterns (graphoepitaxy)[67,86–88] fabricated by top-down lithography or chemical guiding patterns (chemical epitaxy)[89,90] are used to direct the alignment of block copolymer domain. Cylindrical or lamellar alignment has been achieved in block copolymers using DSA with both topographic guiding patterns[86,108–112] and chemical guiding patterns.[113–115] PS-*b*-PtBA (49.3K PS-*b*-PtBA, 76.9% PtBA, PDI = 1.21, P5 in Table 1) after chloroform vapor annealing, which gives cylindrical morphology (Figure 2e), was used as the template to produce a mesoporous silica film with cylindrical channels as shown in Figure 4e. AFM images of the block copolymer films (Figure 8a) showed that most cylinders were oriented parallel to the substrate, which is thermodynamically preferred for thick films, but randomly oriented in-plane. The TEM image (Figure 8b) of the mesoporous silica films also shows an obvious grain boundary after the replication of the block copolymer morphology. The in-plane order improvement in PS-*b*-PtBA templates was investigated using solvents for spin-coating. A mixed solvent,

dx.doi.org/10.1021/ma401018y | *Macromolecules* 2013, 46, 6132–6144

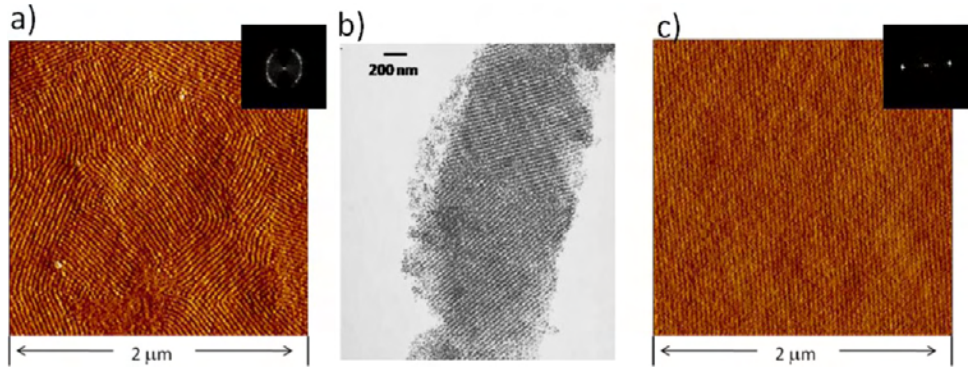

Figure 8. Topography-directed orientation of domains in block copolymer films. (49.3K PS-*b*-PtBA, 76.9% PtBA, PDI = 1.21). (a) AFM phase images of PS-*b*-PtBA film (49.3K PS-*b*-PtBA, 76.9% PtBA, PDI = 1.21) spin-coated from chloroform after solvent annealing (150 μL chloroform in a 250 mL jar) for 15 h. (b) TEM image of the corresponding mesoporous silica film replicated from the polymer template (image a) after supercritical CO_2 infusion and calcination. (c) AFM phase images of PS-*b*-PtBA film (49.3K PS-*b*-PtBA, 76.9% PtBA, PDI = 1.21) spin-coated from 1:1 mixture solvent of toluene and THF after solvent annealing (150 μL chloroform in a 250 mL jar) for 15 h with its Fourier transform image.

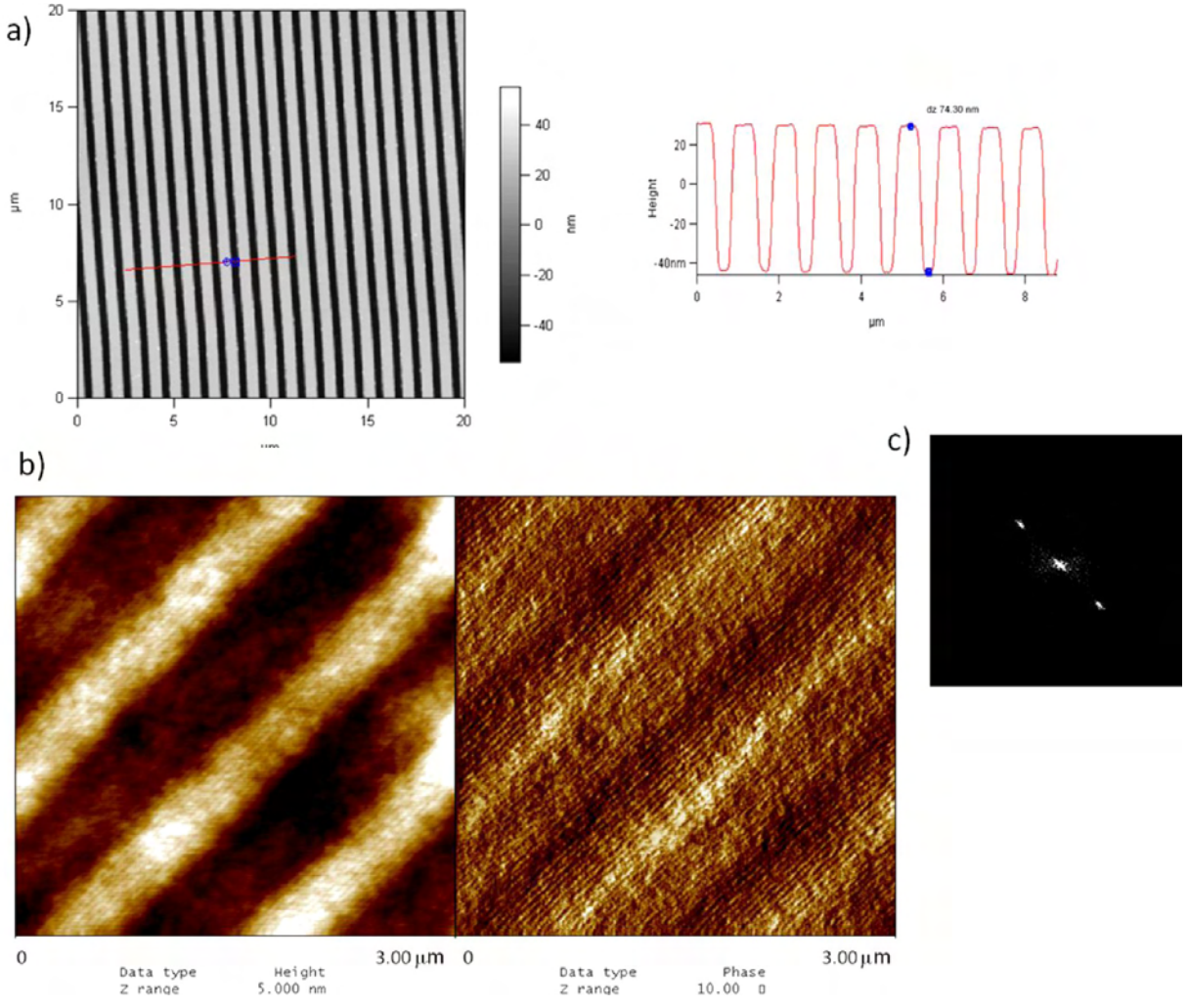

Figure 9. PS-*b*-PtBA block copolymer with cylindrical morphology aligned by an underlying patterned line gratings. (a) AFM height image of the line gratings on the silicon substrate with the thickness 74.3 nm, line-width of 500 nm and pitch length of 1000 nm fabricated by photolithography and AFM profile of the patterned substrate. (b) AFM image of the topography of PS-*b*-PtBA film on the patterned substrate at the scale of 3 μm × 3 μm. (c) Fourier transform of the phase image in part b.

consisting of equal parts THF and toluene, was used in this strategy. Figure 8c and Figure S6 show an increase of the grain size of the cylindrical morphology from less than 1 μm to over 5 μm. This grain size increase is due to the slow evaporation of the mix-solvent relative to chloroform, which reduces the chance of defect generation.

The use of topographic guiding alignment was then investigated in conjunction with slow solvent evaporation to

dx.doi.org/10.1021/ma401018y | *Macromolecules* 2013, 46, 6132−6144

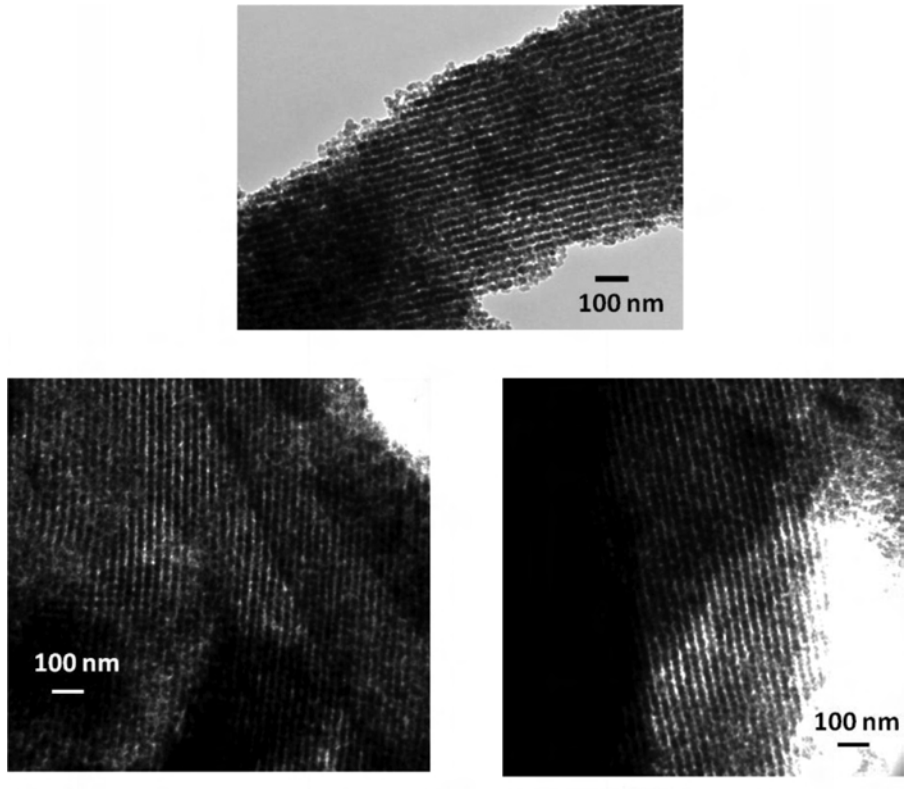

Figure 10. TEM images of mesoporous silica films with aligned channels replicated from block copolymer templates aligned using DSA.

achieve long-range alignment and orientation of the cylinders within PS-*b*-PtBA films. Silicon wafers with oxide thickness 25 nm (line-width 0.201 ± 0.018 μm, pitch length 0.473 ± 0.005 μm), obtained from Lucent Technologies, Inc. were used for DSA. After spin-coating of the same solution used for the films shown in Figure 8c followed by chloroform annealing, the cylinderical domains of the polymer template were guided by the topographical patterns beneath the films as shown in the AFM images (Figure S7a), The long-range alignment of the cylinders was confirmed via Fourier transform (F.T.) of the AFM phase image (Figure S7b).

Additional DSA templates were fabricated in our laboratories. As shown in the Supporting Information (Figure S8), a negative photoresist, NR9−1000PY, was used in the photolithography process. After UV-exposure, development, reactive ionic etching (RIE) using CF_4, and cleaning, patterned substrates with the line-widths as small as 500 nm and period of 1 μm were fabricated. The depth of the line patterns was tuned by changing the RIE time. Patterned line gratings on silicon wafers with depths of 75 nm were fabricated after etching under CF_4 for 8 min. (Figure 9a) A PS-*b*-PtBA film with a thickness of approximately 180 nm was spin-coated from a solution of 3 wt % PS-*b*-PtBA in THF: Toluene (1:1 weight ratio) onto the patterned substrate. Very well aligned cylinders were again achieved after overnight chloroform annealing. AFM characterization of the aligned film (3 μm by 3 μm) is shown in (Figure 9b) and also in Supporting Information (Figure S9) for a 6 μm by 6 μm region. After replication of the template in supercritical CO_2 and 400 °C calcination, TEM was used to characterize the final structures of the mesoporous silica films. TEM images in Figure 10 show that well aligned channels were successfully replicated in the mesoporous silica films. However, due to the fact that microscopy methods provide information over relatively small areas, we used grazing-incidence small-angle X-ray scattering (GISAXS) to provide information regarding large-area alignment. The sample was placed on a rotatable stage and aligned with X-ray beam at an angle, known as the grazing incidental angle (α) (Supporting Information Figure S10), which is between the critical angles of the polymer films (or mesoporous silica films) and silicon substrates to give strongest scattering signal across the whole film thickness. The bare lithographically patterned line gratings on the silicon substrate produced anisotropic scattering patterns on the GISAXS spectrum during rotation of the stage (ϕ) as shown in Supporting Information (Figure S10) that must be accounted for (Figure 11). Intense scattering patterns arranged in an arc around the beam center were observed in the spectrum when the beam was exactly parallel to the lithographically patterned line gratings; we define the relative ϕ value as 0 at this rotation (Figure 11c). When the stage was rotated by 90° to render the X-ray perpendicular to the line gratings, a series of circular patterns line up in the q-z axes (Figure S14, parts d−f). However, if the stage was rotated by only a very small angle away from the parallel direction, about 2° in either direction, the circular scattering patterns moved away from the center and are rearranged as a tail emanating from the beam stop as shown in Figure 11, parts b and d. The diffraction from grating has been studied previously by couple research groups.[116,117] We also used modeling to quantitatively describe the GISAXS-geometry scattering from the substrate with the lithographically patterned gratings as shown in the Supporting Information section. The results are shown in Figure 11f for different relative rotation angles, and match very well with the experimental results of the scattering from patterned gratings in Figures 11, parts a−e.

The same theory can also be applied to the scattering from the mesoporous silica films fabricated on top of the patterned silicon

dx.doi.org/10.1021/ma401018y | *Macromolecules* 2013, 46, 6132−6144

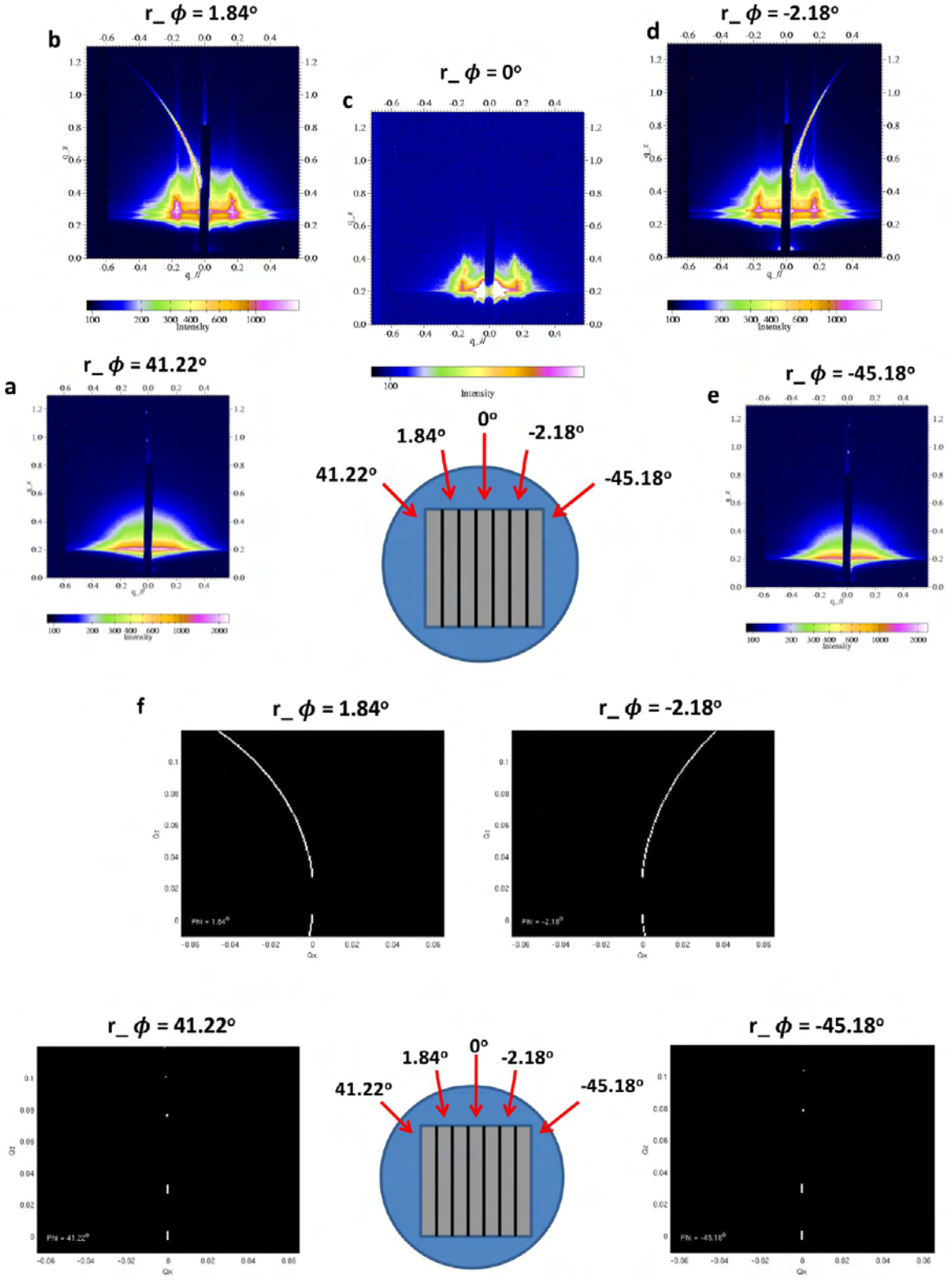

Figure 11. (a–e) GISAXS spectra for silica films with aligned cylindrical pore with different relative ϕ during azimuthal rotation of the sample stage. (f) Modeling results of GISAXS geometry scattering from the substrate with lithographically patterned gratings during azimuthal rotation of the sample stage.

gratings. When the beam was parallel to the line gratings underneath, the scattering intensity from mesoporous silica film was apparent in the $q_{\|}$ direction, with a d-spacing of 35 nm (Figure 11c). As the stage was rotated by a very small angle, such as 2°, either counter clockwise or clockwise, the scattering from the mesoporous films became much more obvious, as shown in Figure 11, parts b and d, because of the attenuation of the background scattering from the substrate line gratings. However, if the stage was rotated by a larger angle of approximately 45°, no scattering from the mesoporous silica film was observed in Figure

dx.doi.org/10.1021/ma401018y | *Macromolecules* 2013, 46, 6132–6144

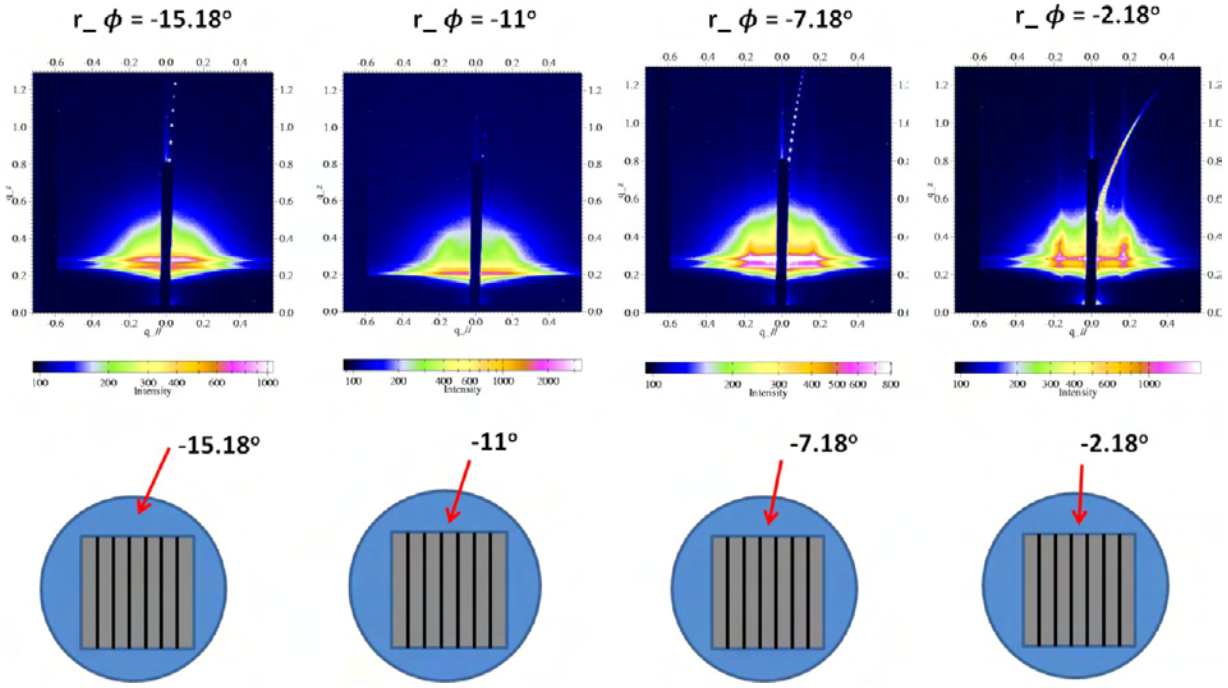

Figure 12. Sharp transition of the scattering from mesoporous silica films during azimuthal rotation of the sample stage with small angles.

11, parts a and e, which indicates a lack of contrast in $q_{\|}$ direction. The anisotropic scattering patterns from mesoporous silica films indicates that the mesochannels in mesoporous silica films are all aligned in a parallel manner with the underlying gratings, and thus scattering patterns from mesoporous films was only observed in $q_{\|}$ when the X-ray beam was colinear with the line gratings.

In order to confirm good alignment of the mesochannels within the film, the sharpness of the anisotropic transition for the scattering from the mesoporous silica film needs to be determined while rotating the stage at small angles (Figure 12). When the relative rotation angle (r_ϕ) increased from 2° to 15°, the scattering from the mesoporous silica film decreased dramatically as shown in Figure 12. This sharp transition indicates that the cylindrical mesochannels within the mesoporous silica film were well-aligned in the direction parallel to the underlying line gratings. The long-range alignment can be quantified using the angular spread as reported in literature.[68,118,119] Scattering intensity versus azimuthal angle relation curve is shown in the Supporting Information (Figure S11), which gives the angular spread $\Delta\theta_{hwhm}$ (half width at half-maximum) ≈ 5.5. Similarly, the GISAXS method was also applied to block copolymer template PS-*b*-PtBA after solvent annealing but before silica infusion. As shown in Supporting Information (Figure S12), the similar alignment as that found in the mesoporous silica film was observed, although the scattering intensity was not as strong due to the weaker electron density contrast between PS and PtBA in comparison to that between air and silica. Additional control experiments were conducted to determine the reliability of the GISAXS measurements for the long-range alignment as shown in Supporting Information (Figures S13 and S14).

CONCLUSIONS

A method to fabricate mesoporous silica films with large pores of tunable geometry is presented. Excellent control of film structure was possible due to the separation of template preparation, precursor infusion and silica condensation into discrete steps. The template morphology was controlled by varying the molecular weight, volume fractions of the segments, and PDI of the block copolymer and by controlling film thickness and annealing conditions. Structures developed in the template by manipulation of these variables, including FCC spherical packing, an uncommonly accessed morphology in phase diagram, were successively conveyed to the mesoporous films. Large pores in mesoporous silica films were accessible by increasing both the molecular weight and the PDI of the template. Pore orientation in films containing cylindrical pores was controlled by adjusting template film thickness. Finally, alignment of cylindrical pores in mesoporous silica films was successfully achieved by applying directed self-assembly on the block copolymer templates. Such precise control of morphology in mesoporous silica films is expected to enhance their utility in a broad range of applications.

ASSOCIATED CONTENT

Supporting Information

GISAXS spectra/integrations and TEM image of mesoporous silica films templated from P1, P2, P3, P4, and P5 (Table 1), AFM phase image at the scale of 5 μm × 5 μm of PS-*b*-PtBA film (49.3K PS-*b*-PtBA, 76.9% PtBA, PDI = 1.21) spin-coated from mixture solvent of Toluene and THF after solvent annealing with its Fourier Transform image, AFM image of the topography of PS-*b*-PtBA film on the patterned substrate (with oxide pattern thickness of 25 nm, linewidth of 0.201 ± 0.018 μm, and pitch length of 0.473 ± 0.005 μm from Lucent Technologies, Inc.) with the Fourier Transform of the phase image; schematic illustration of photolithography for patterned substrate fabrication, AFM image of the topography of PS-*b*-PtBA film on the patterned substrate at the scale of 6 μm × 6 μm with its Fourier transform image, GISAXS set up for anisotropic substrate, plot of scattering intensity of the first order peak in GISAXS 1D profile versus azimuthal angle, GISAXS spectra of aligned PS-*b*-PtBA films before supercritical fluid infusion during azimuthal rotation

dx.doi.org/10.1021/ma401018y | *Macromolecules* 2013, 46, 6132−6144

of the sample stage, AFM height images of the patterned substrate silicon wafers (Control I, Control II) fabricated by photolithography, AFM profiles of the patterned substrate AFM images of the topography of PS-*b*-PtBA film on the patterned substrates (Control I, Control II); GISAXS spectra for the mesoporous silica films on three substrates (Control I, standard, Control II), when beam direction is parallel to the underneath line-patterns and orthogonal to the underlying substrate patterns, and modeling of scattering from topographically patterned wafers. This material is available free of charge via the Internet at http://pubs.acs.org.

AUTHOR INFORMATION

Corresponding Author

*Corresponding Author. E-mail: watkins@polysci.umass.edu.

Notes

The authors declare no competing financial interest.

ACKNOWLEDGMENTS

This work was supported by the NSF Center for Hierarchical Manufacturing (CMMI-1025020). Facilities were supported by the Cornell High Energy Synchrotron Source (CHESS) G1 station, a national user facility supported by the National Science Foundation and the National Institutes of Health/National Institute of General Medical Sciences under Award No. DMR-0936384. Facilities supported by the Materials Research Science and Engineering Center at University of Massachusetts—Amherst were used in this work. We thank Dr. Dhanasekaran Thirunavukkarasu and Mr. Louis Raboin for assistance with characterization and Dr. John Ell, Dr. Nick Hendricks, and Todd Crosby for helpful discussions.

REFERENCES

(1) Innocenzi, P.; Malfatti, L. *Chem. Soc. Rev.* **2013**, *42*, 4198−4216.
(2) Zhu, Y.; Müller, T. E.; Lercher, J. A. *Adv. Funct. Mater.* **2008**, *18*, 3427−3433.
(3) Volksen, W.; Miller, R. D.; Dubois, G. *Chem. Rev.* **2009**, *110*, 56−110.
(4) Wang, Z.; Wang, H.; Mitra, A.; Huang, L.; Yan, Y. *Adv. Mater.* **2001**, *13*, 746−749.
(5) Seraji, S.; Wu, Y.; Forbess, M.; Limmer, S. J.; Chou, T.; Cao, G. Z. *Adv. Mater.* **2000**, *12*, 1695−1698.
(6) Baskaran, S.; Liu, J.; Domansky, K.; Kohler, N.; Li, X.; Coyle, C.; Fryxell, G. E.; Thevuthasan, S.; Williford, R. E. *Adv. Mater.* **2000**, *12*, 291−294.
(7) Crossland, E. J. W.; Nedelcu, M.; Ducati, C.; Ludwigs, S.; Hillmyer, M. A.; Steiner, U.; Snaith, H. J. *Nano Lett.* **2008**, *9*, 2813−2819.
(8) Crossland, E. J. W.; Kamperman, M.; Nedelcu, M.; Ducati, C.; Wiesner, U.; Smilgies, D. M.; Toombes, G. E. S.; Hillmyer, M. A.; Ludwigs, S.; Steiner, U.; Snaith, H. J. *Nano Lett.* **2008**, *9*, 2807−2812.
(9) Jose, R.; Thavasi, V.; Ramakrishna, S. *J. Am. Ceram. Soc.* **2009**, *92*, 289−301.
(10) O'Regan, B.; Gratzel, M. *Nature* **1991**, *353*, 737−740.
(11) Park, D.-H.; Nishiyama, N.; Egashira, Y.; Ueyama, K. *Ind. Eng. Chem. Res.* **2001**, *40*, 6105−6110.
(12) Guliants, V. V.; Carreon, M. A.; Lin, Y. S. *J. Membr. Sci.* **2004**, *235*, 53−72.
(13) Joo, J.; Shim, J.; Seo, H.; Jung, N.; Wiesner, U.; Lee, J.; Jeon, S. *Anal. Chem.* **2010**, *82*, 3032−3037.
(14) Ogawa, M.; Kuroda, K.; Mori, J.-i. *Chem. Commun.* **2000**, 2441−2442.
(15) Kageyama, K.; Tamazawa, J.-i.; Aida, T. *Science* **1999**, *285*, 2113−2115.
(16) Liu, A. M.; Hidajat, K.; Kawi, S.; Zhao, D. Y. *Chem. Commun.* **2000**, 1145−1146.
(17) Nooney, R. I.; Kalyanaraman, M.; Kennedy, G.; Maginn, E. J. *Langmuir* **2000**, *17*, 528−533.
(18) Liu, X.; Wang, R.; Xia, Y.; He, Y.; Zhang, T. *Sens. Lett.* **2011**, *9*, 698−702.
(19) Domansky, K.; Liu, J.; Wang, L.-Q.; Engelhard, M. H.; Baskaran, S. *J. Mater. Res.* **2001**, *16*, 2810−2816.
(20) Gomez-Vega, J. M.; Iyoshi, M.; Kim, K. Y.; Hozumi, A.; Sugimura, H.; Takai, O. *Thin Solid Films* **2001**, 615−620.
(21) Wang, X.-P.; Li, X.; Onuma, K.; Ito, A.; Sogo, Y.; Kosuge, K.; Oyane, A. *J. Mater. Chem.* **2010**, *20*, 6437−6445.
(22) Li, X.; Wang, X.; He, D.; Shi, J. *J. Mater. Chem.* **2008**, *18*, 4103−4109.
(23) Alberius, P. C. A.; Frindell, K. L.; Hayward, R. C.; Kramer, E. J.; Stucky, G. D.; Chmelka, B. F. *Chem. Mater.* **2002**, *14*, 3284−3294.
(24) Bagshaw, S. A.; Prouzet, E.; Pinnavaia, T. J. *Science* **1995**, *269*, 1242.
(25) Attard, G. S.; Glyde, J. C.; Goltner, C. G. *Nature* **1995**, *378*, 366−368.
(26) Templin, M.; Franck, A.; Du Chesne, A.; Leist, H.; Zhang, Y.; Ulrich, R.; Schadler, V.; Wiesner, U. *Science* **1997**, *278*, 1795.
(27) Zhao, D.; Chmelka, B. F.; Stucky, G. D. *Science* **1998**, *279*, 548.
(28) Lu, Y.; Fan, H.; Stump, A.; Ward, T. L.; Rieker, T.; Brinker, C. J. *Nature* **1999**, *398*, 223.
(29) Göltner, C. G.; Henke, S.; Weissenberger, M. C.; Antonietti, M. *Angew. Chem., Int. Ed.* **1998**, *37*, 613−616.
(30) Honma, I.; Zhou, H. S.; Kundu, D.; Endo, A. *Adv. Mater.* **2000**, *12*, 1529−1533.
(31) Klotz, M.; Ayral, A.; Guizard, C.; Cot, L. *J. Mater. Chem.* **2000**, *10*, 663−669.
(32) Deng, Y.; Yu, T.; Wan, Y.; Shi, Y.; Meng, Y.; Gu, D.; Zhang, L.; Huang, Y.; Liu, C.; Wu, X.; Zhao, D. *J. Am. Chem. Soc.* **2007**, *129*, 1690−1697.
(33) Huang, L.; Yan, X.; Kruk, M. *Langmuir* **2010**, *26*, 14871−14878.
(34) Ma, G.; Yan, X.; Li, Y.; Xiao, L.; Huang, Z.; Lu, Y.; Fan, J. *J. Am. Chem. Soc.* **2010**, *132*, 9596−9597.
(35) Chen, L.; Zhu, G.; Zhang, D.; Zhao, H.; Guo, M.; Shi, W.; Qiu, S. *J. Mater. Chem.* **2009**, *19*, 2013−2017.
(36) Boissiere, C.; Grosso, D.; Chaumonnot, A.; Nicole, L.; Sanchez, C. *Adv. Mater.* **2011**, *23*, 599−623.
(37) Guillemot, F.; Brunet-Bruneau, A.; Bourgeat-Lami, E.; Gacoin, T.; Barthel, E.; Boilot, J. P. *Chem. Mater.* **2010**, *22*, 2822−2828.
(38) Rühle, B.; Davies, M.; Lebold, T.; Bräuchle, C.; Bein, T. *ACS Nano* **2012**, *6*, 1948−1960.
(39) Fan, R.; Huh, S.; Yan, R.; Arnold, J.; Yang, P. *Nat. Mater.* **2008**, *7*, 303−307.
(40) Kirstein, J.; Platschek, B.; Jung, C.; Brown, R.; Bein, T.; Brauchle, C. *Nat. Mater.* **2007**, *6*, 303−310.
(41) Wu, C.-W.; Ohsuna, T.; Edura, T.; Kuroda, K. *Angew. Chem., Int. Ed.* **2007**, *46*, 5364−5368.
(42) Pai, R. A.; Humayun, R.; Schulberg, M. T.; Sengupta, A.; Sun, J.-N.; Watkins, J. J. *Science* **2004**, *303*, 507−510.
(43) Pai, R. A.; Watkins, J. J. *Adv. Mater.* **2006**, *18*, 241−245.
(44) Gupta, R. R.; RamachandraRao, V. S.; Watkins, J. J. *Macromolecules* **2003**, *36*, 1295−1303.
(45) Gupta, R. R.; Lavery, K. A.; Francis, T. J.; Webster, J. R. P.; Smith, G. S.; Russell, T. P.; Watkins, J. J. *Macromolecules* **2002**, *36*, 346−352.
(46) Nagarajan, S.; Li, M.; Pai, R. A.; Bosworth, J. K.; Busch, P.; Smilgies, D. M.; Ober, C. K.; Russell, T. P.; Watkins, J. J. *Adv. Mater.* **2008**, *20*, 246−251.
(47) Chen, H.-T.; Crosby, T. A.; Park, M.-H.; Nagarajan, S.; Rotello, V. M.; Watkins, J. J. *J. Mater. Chem.* **2009**, *19*, 70−74.
(48) Nagarajan, S.; Bosworth, J. K.; Ober, C. K.; Russell, T. P.; Watkins, J. J. *Chem. Mater.* **2007**, *20*, 604−606.
(49) Nagarajan, S.; Russell, T. P.; Watkins, J. J. *Adv. Funct. Mater.* **2009**, *19*, 2728−2734.
(50) Bates, F. S. *Science* **1991**, *251*, 898−905.
(51) Kim, S.; Briber, R. M.; Karim, A.; Jones, R. L.; Kim, H. C. *Macromolecules* **2007**, *40*, 4102−4105.
(52) Niu, S.; Saraf, R. F. *Macromolecules* **2003**, *36*, 2428−2440.

(53) Zhou, S.; Chu, B. *Macromolecules* **1998**, *31*, 7746−7755.
(54) Buhler, E.; Dobrynin, A. V.; DeSimone, J. M.; Rubinstein, M. *Macromolecules* **1998**, *31*, 7347−7355.
(55) Albert, J. N. L.; Bogart, T. D.; Lewis, R. L.; Beers, K. L.; Fasolka, M. J.; Hutchison, J. B.; Vogt, B. D.; Epps, T. H. *Nano Lett.* **2011**, *11*, 1351−1357.
(56) Phillip, W. A.; Hillmyer, M. A.; Cussler, E. L. *Macromolecules* **2010**, *43*, 7763−7770.
(57) van Zoelen, W.; Asumaa, T.; Ruokolainen, J.; Ikkala, O.; ten Brinke, G. *Macromolecules* **2008**, *41*, 3199−3208.
(58) Bang, J.; Kim, B. J.; Stein, G. E.; Russell, T. P.; Li, X.; Wang, J.; Kramer, E. J.; Hawker, C. J. *Macromolecules* **2007**, *40*, 7019−7025.
(59) Cavicchi, K. A.; Berthiaume, K. J.; Russell, T. P. *Polymer* **2005**, *46*, 11635−11639.
(60) Kim, S. H.; Misner, M. J.; Xu, T.; Kimura, M.; Russell, T. P. *Adv. Mater.* **2004**, *16*, 226−231.
(61) Russell, T. P.; Coulon, G.; Deline, V. R.; Miller, D. C. *Macromolecules* **1989**, *22*, 4600−4606.
(62) Green, P. F.; Christensen, T. M.; Russell, T. P. *Macromolecules* **1991**, *24*, 252−255.
(63) Mayes, A. M.; Russell, T. P.; Bassereau, P.; Baker, S. M.; Smith, G. S. *Macromolecules* **1994**, *27*, 749−755.
(64) Smith, A. P.; Sehgal, A.; Douglas, J. F.; Karim, A.; Amis, E. J. *Macromol. Rapid Commun.* **2003**, *24*, 131−135.
(65) Han, E.; Stuen, K. O.; Leolukman, M.; Liu, C.-C.; Nealey, P. F.; Gopalan, P. *Macromolecules* **2009**, *42*, 4896−4901.
(66) Choi, S.; Kim, E.; Ahn, H.; Naidu, S.; Lee, Y.; Ryu, D. Y.; Hawker, C. J.; Russell, T. P. *Soft Matter.* **2012**, *8*, 3463−3469.
(67) Kim, H.-C.; Park, S.-M.; Hinsberg, W. D. *Chem. Rev.* **2009**, *110*, 146−177.
(68) Hong, S. W.; Huh, J.; Gu, X.; Lee, D. H.; Jo, W. H.; Park, S.; Xu, T.; Russell, T. P. *Proc. Natl. Acad. Sci. U.S.A.* **2012**, *109*, 1402−1406.
(69) Park, S.; Lee, D. H.; Xu, J.; Kim, B.; Hong, S. W.; Jeong, U.; Xu, T.; Russell, T. P. *Science* **2009**, *323*, 1030−1033.
(70) Cheng, J. Y.; Mayes, A. M.; Ross, C. A. *Nat. Mater.* **2004**, *3*, 823−828.
(71) Sundrani, D.; Darling, S. B.; Sibener, S. J. *Nano Lett.* **2004**, *4*, 273−276.
(72) Sundrani, D.; Darling, S. B.; Sibener, S. J. *Langmuir* **2004**, *20*, 5091−5099.
(73) Sundrani, D.; Sibener, S. J. *Macromolecules* **2002**, *35*, 8531−8539.
(74) Park, S. M.; Stoykovich, M. P.; Ruiz, R.; Zhang, Y.; Black, C. T.; Nealey, P. F. *Adv. Mater.* **2007**, *19*, 607−611.
(75) Ruiz, R.; Ruiz, N.; Zhang, Y.; Sandstrom, R. L.; Black, C. T. *Adv. Mater.* **2007**, *19*, 2157−2162.
(76) Son, J. G.; Hannon, A. F.; Gotrik, K. W.; Alexander-Katz, A.; Ross, C. A. *Adv. Mater.* **2011**, *23*, 634−639.
(77) Ashok, B.; Muthukumar, M.; Russell, T. P. *J. Chem. Phys.* **2001**, *115*, 1559−1564.
(78) Xu, T.; Zhu, Y.; Gido, S. P.; Russell, T. P. *Macromolecules* **2004**, *37*, 2625−2629.
(79) Thurn-Albrecht, T.; DeRouchey, J.; Russell, T. P.; Kolb, R. *Macromolecules* **2002**, *35*, 8106−8110.
(80) DeRouchey, J.; Thurn-Albrecht, T.; Russell, T. P.; Kolb, R. *Macromolecules* **2004**, *37*, 2538−2543.
(81) Lyakhova, K. S.; Zvelindovsky, A. V.; Sevink, G. J. A. *Macromolecules* **2006**, *39*, 3024−3037.
(82) Morkved, T. L.; Urbas, A. M.; Ehrichs, E. E. *Science* **1996**, *273*, 931−931.
(83) Wang, J.-Y.; Chen, W.; Russell, T. P. *Macromolecules* **2008**, *41*, 7227−7231.
(84) Wang, J.-Y.; Leiston-Belanger, J. M.; Sievert, J. D.; Russell, T. P. *Macromolecules* **2006**, *39*, 8487−8491.
(85) Kim, H.-C.; Park, S.-M.; Hinsberg, W. D. *Chem. Rev.* **2010**, *110*, 146−177.
(86) Sundrani, D.; Darling, S. B.; Sibener, S. J. *Nano Lett.* **2004**, *4*, 273−276.
(87) Park, S.; Lee, D. H.; Xu, J.; Kim, B.; Hong, S. W.; Jeong, U.; Xu, T.; Russell, T. P. *Science* **2009**, *323*, 1030−1033.
(88) Cheng, J. Y.; Mayes, A. M.; Ross, C. A. *Nat. Mater.* **2004**, *3*, 823−828.
(89) Stoykovich, M. P.; Muller, M.; Kim, S. O.; Solak, H. H.; Edwards, E. W.; de Pablo, J. J.; Nealey, P. F. *Science* **2005**, *308*, 1442−1446.
(90) Xu, J.; Park, S.; Wang, S.; Russell, T. P.; Ocko, B. M.; Checco, A. *Adv. Mater.* **2010**, *22*, 2268−2272.
(91) Davis, K. A.; Charleux, B.; Matyjaszewski, K. *J. Polym. Sci. A Polym. Chem.* **2000**, *38*, 2274−2283.
(92) Romang, A. H.; Watkins, J. J. *Chem. Rev.* **2009**, *110*, 459−478.
(93) Tirumala, V. R.; Pai, R. A.; Agarwal, S.; Testa, J. J.; Bhatnagar, G.; Romang, A. H.; Chandler, C.; Gorman, B. P.; Jones, R. L.; Lin, E. K.; Watkins, J. J. *Chem. Mater.* **2007**, *19*, 5868−5874.
(94) Lynd, N. A.; Meuler, A. J.; Hillmyer, M. A. *Prog. Polym. Sci.* **2008**, *33*, 875−893.
(95) Sides, S. W.; Fredrickson, G. H. *J. Chem. Phys.* **2004**, *121*, 4974−4986.
(96) Cooke, D. M.; Shi, A.-C. *Macromolecules* **2006**, *39*, 6661−6671.
(97) van Dijk, M. A.; van den Berg, R. *Macromolecules* **1995**, *28*, 6773−6778.
(98) Suh, K. Y.; Kim, Y. S.; Lee, H. H. *J. Chem. Phys.* **1998**, *108*, 1253−1256.
(99) Matsen, M. W.; Bates, F. S. *Macromolecules* **1996**, *29*, 1091−1098.
(100) Semenov, A. N. *Macromolecules* **1989**, *22*, 2849−2851.
(101) Matsen, M. W.; Bates, F. S. *J. Chem. Phys.* **1997**, *106*, 2436−2448.
(102) Sakamoto, N.; Hashimoto, T.; Han, C. D.; Kim, D.; Vaidya, N. Y. *Macromolecules* **1997**, *30*, 1621−1632.
(103) Sakamoto, N.; Hashimoto, T. *Macromolecules* **1998**, *31*, 8493−8502.
(104) Dormidontova, E. E.; Lodge, T. P. *Macromolecules* **2001**, *34*, 9143−9155.
(105) Huang, Y.-Y.; Hsu, J.-Y.; Chen, H.-L.; Hashimoto, T. *Macromolecules* **2007**, *40*, 406−409.
(106) Lodge, T. P.; Bang, J.; Park, M. J.; Char, K. *Phys. Rev. Lett.* **2004**, *92*, 145501.
(107) Matsen, M. W. *J. Phys.: Condens. Matter* **2002**, *14*, R21−R47.
(108) Sundrani, D.; Darling, S. B.; Sibener, S. J. *Langmuir* **2004**, *20*, 5091−5099.
(109) Sundrani, D.; Sibener, S. J. *Macromolecules* **2002**, *35*, 8531−8539.
(110) Park, S.-M.; Stoykovich, M. P.; Ruiz, R.; Zhang, Y.; Black, C. T.; Nealey, P. F. *Adv. Mater.* **2007**, *19*, 607−611.
(111) Ruiz, R.; Ruiz, N.; Robert, Y. Z.; Sandstrom, L.; Black, C. T. *Adv. Mater.* **2007**, *19*, 2157−2162.
(112) Son, J. G.; Hannon, A. F.; Gotrik, K. W.; Alexander-Katz, A.; Ross, C. A. *Adv. Mater.* **2011**, *23*, 634−639.
(113) Kim, S. O.; Solak, H. H.; Stoykovich, M. P.; Ferrier, N. J.; de, P. J. J.; Nealey, P. F. *Nature* **2003**, *424*, 411−414.
(114) Stoykovich, M. P.; Mueller, M.; Kim, S. O.; Solak, H. H.; Edwards, E. W.; de, P. J. J.; Nealey, P. F. *Science* **2005**, *308*, 1442−1446.
(115) Ruiz, R.; Kang, H.; Detcheverry, F. A.; Dobisz, E.; Kercher, D. S.; Albrecht, T. R.; de, P. J. J.; Nealey, P. F. *Science* **2008**, *321*, 936−939.
(116) Yan, M.; Gibaud, A. *J. Appl. Crystallogr.* **2007**, *40*, 1050−1055.
(117) Rueda, D. R.; Martín-Fabiani, I.; Soccio, M.; Alayo, N.; Pérez-Murano, F.; Rebollar, E.; García-Gutiérrez, M. C.; Castillejo, M.; Ezquerra, T. A. *J. Appl. Crystallogr.* **2012**, *45*, 1038−1045.
(118) Singh, G.; Yager, K. G.; Berry, B.; Kim, H.-C.; Karim, A. *ACS Nano* **2012**, *6*, 10335−10342.
(119) Tang, C.; Tracz, A.; Kruk, M.; Zhang, R.; Smilgies, D.-M.; Matyjaszewski, K.; Kowalewski, T. *J. Am. Chem. Soc.* **2005**, *127*, 6918−6919.